JET-R(96)06

SOL-One
A One-D Scrape-Off-Layer Transport Code

G T A Huysmans, K Borrass[1].

JET Joint Undertaking, Abingdon, Oxfordshire, OX14 3EA, UK.
[1] Present Affiliation: Max-Planck Institut für Plasmaphysik,
Garching bei München, Germany.

July 1996

1. INTRODUCTION AND BASIC CONCEPT

The numerical code SOL-One has been developed to enable the study of different regimes of divertor plasmas in a simplified one dimensional geometry. The objectives of the code are to solve the full time evolution of the scrape-off layer (SOL) equations. Also, to study various different models the equations are implemented in a transparent way such that the equations can be easily adjusted.

The model basically comprises a fluid description of a hydrogenic SOL plasma and of background neutrals. The equations adopted for describing the transport in the scrape-off (SOL) are derived from the general equations for conservation of particles momentum and energy [1] with the following simplifications made:

(i) A simplified geometry as outlined in Fig. 1 is used (slab geometry with constant pitch). z is the coordinate along $\vec{B}$, with the stagnation point being the origin, x is the transverse coordinate which is removed by averaging. Because of axisymmetry all quantities depend (apart from x) only on the distance from the plate. However, in order to simplify the presentation of data, we use z as a label throughout instead of $\tilde{y}$. At certain points in the derivation of the equations it will also be convenient to use the coordinate systems $\left(\tilde{e}_{\tilde{y}}, \tilde{e}_{\tilde{z}}\right)$ and $\left(\tilde{e}_{\tilde{y}}, \tilde{e}_{z}\right)$ alternatively.

(ii) For the ions transverse transport inside a flux surface is neglected. The plasma equations are averaged with respect to the transverse direction (x -direction, 1-D model), assuming negligible particle, momentum and power fluxes to the wall.

(iii) The high collisionality limit with respect to i-n collisions (elastic and charge exchange, cx) (*Fluid Limit*) is considered in the present version. This implies:

- After a few collisions slow neutrals are heated up and hence can only exist in the immediate vicinity of the plate. Hence only fast neutrals (in what follows simply called neutrals) have to be considered.

- $T_i = T_0$ and as far as energy transport is concerned ions and neutrals can be treated as one fluid.

- If $\lambda_{i-n} << \ell^*$, where λ_{i-n} is the ion-neutral collision length and ℓ^* is the poloidal width of the recyling zone, also transverse, neutrals induced transport is negligible and a 1-D approximation can be applied by analogy with the ions.

However, different from the ions two independent components of the neutral momentum

balance have to be considered. (Along $\vec{B}$ and in the poloidal direction.)

The variables under consideration are the ion and neutral densities n_i, n_o, the ion and electron temperature T_i and T_e, the ion velocities, v_i, and two neutral velocities.

In Sections 2 to 4 the general underlying physics is described. The coefficients are described that are of universal character. Sources or transport coefficients which have model character by themselves or may be subject to alteration for various code options, are considered in Appendix I.

Besides the very high collisionality limit for neutrals, the long mean free path limit has also been implemented. In the long mean free path limit neutrals collide mainly with the wall, losing energy and momentum with each collision. The neutral gas experienced by the plasma ions is therefore formed by neutrals that have not yet undergone an ion collision after their last wall impact. It is a mixture of reflected atoms, molecules and Frank Condon atoms, which we characterise by some average temperature T_0 and prescribe as input parameter. Wall collisions exert a force on the neutrals, which is taken into account in the neutral momentum balances. The particle balance is unchanged in relation to the fluid limit. Transition to the long mean free path limit is relatively straight forward and will not be dealt with in this report.

In Section 5, the numerical algorithms used in the code, i.e. Petrov-Galerkin finite elements and implicit time stepping are discussed. Finally, as a first application, the detachment of the divertor plasma in a static gas target is studied in Section 6.

2. DESCRIPTION OF UNDERLYING PHYSICS

2.1 2-D Plasma Equations

Ion Continuity Equation

$$\frac{\partial n_i}{\partial t} = -\frac{\partial}{\partial z}\left(n_i v_{i,z}\right) + \frac{\partial}{\partial x}\left(D_\perp \frac{\partial n_i}{\partial x}\right) + S_{fuel} + n_0 n_i \left(S_i - S_{rec}\right) \qquad (1)$$

where S_i is the ionisation rate, S_{fuel} is a source of ions associated with external particle sources and $D_\perp$ is the perpendicular diffusion coefficient.[1]

Ion Momentum Balance (z-Direction)

$$\frac{\partial n_i m v_{i,z}}{\partial t} = -\frac{\partial}{\partial z}\left[n_i\left(T_e + T_i\right) + n_i m v_{i,z}^2\right]$$

---

[1] The hydrogen atomic physics is described in Appendix 2.

$$+1.28\frac{\partial}{\partial z}\left(nT_i\tau_i\frac{\partial \upsilon_{i,z}}{\partial z}\right)+\frac{\partial}{\partial x}\left(m\upsilon_i D_\perp\frac{\partial n_i}{\partial x}\right)+R_{i-n,z} \qquad (2)$$

$\vec{R}_{i-n}$ describes the momentum exchange with neutrals due to ionisation, charge exchange and elastic i-n collisions.

$$R_{i-n,z}=\vec{e}_z\cdot\left(mn_in_0\left(S_i\vec{\upsilon}_0-S_{rec}\vec{\upsilon}_i\right)+mn_in_0\left(S_{cx}+\upsilon_t\sigma_{i-n}\right)\left(\vec{\upsilon}_0-\vec{\upsilon}_i\right)\right) \qquad (3)$$

where S_i and S_{cx} are the ionisation and charge exchange rates, respectively, σ_{i-n} is the elastic i-n collision cross-section and υ_t is the ion thermal velocity. τ_i is the Braginskii ion collision frequency.[2]

Ion Energy Equation $\left(E_i=\frac{3}{2}n_iT_i+\frac{1}{2}mn_i\upsilon_{i,z}^2\right)$

$$\frac{\partial E_i}{\partial t}=-\frac{\partial}{\partial z}\left[n_i\upsilon_{i,z}\left(\frac{5}{2}T_i+\frac{1}{2}m\upsilon_{i,z}^2\right)-n_i\chi_{\|,i}\frac{\partial T_i}{\partial z}\right]-\upsilon_{i,z}\frac{\partial n_iT_e}{\partial z}$$

$$+\frac{\partial}{\partial x}\left[n_i\chi_{\perp,i}\frac{\partial T_i}{\partial x}+\left(\frac{5}{2}T_i+\frac{1}{2}m\upsilon_{i,z}^2\right)D_\perp\frac{\partial n_i}{\partial x}\right]-Q_{\Delta,e}+Q_{0,i} \qquad (4)$$

$Q_{0,i}$ is the ion-neutral heat transfer which need not be specified (see below). The electron-ion heat transfer is given by [1]

$$Q_{\Delta,e}=-\frac{n_i}{\tau_e}\frac{3m_e}{m}(T_e-T_i)$$

Classical parallel ion heat diffusivity is assumed [1]

$$\chi_{\|,i}=3.9\frac{T_i\tau_i}{m}\qquad \tau_i=\frac{3\sqrt{m}T_i^{\frac{3}{2}}}{4\sqrt{\pi}\lambda e^4z^4n_i}$$

where λ is the Coulomb logarithm. Perpendicular ion heat transport is small compared to the typical anomalous convective heat transport and is neglected $\left(\chi_{\perp,i}=0\right)$.

Electron Temperature Equation $\left(E_e=\frac{3}{2}n_iT_e\right)$

---

[2] Frequently used terms are summarised in Appendix 1.

$$\frac{\partial E_e}{\partial t} = -\frac{\partial}{\partial z}\left[\frac{5}{2}T_e n_i \upsilon_{i,z} - n_i \chi_{\|,e}\frac{\partial T_e}{\partial z}\right] + \frac{\partial}{\partial x}\left[\frac{5}{2}T_e D_{\perp,e}\frac{\partial n_i}{\partial x} + n_i \chi_{\perp,e}\frac{\partial T_e}{\partial x}\right]$$

$$+\upsilon_{i,z}\frac{\partial(n_i T_e)}{\partial z} + Q_{\Delta,e} + Q_i \qquad (5)$$

Q_i is the ionisation loss:

$$Q_i = -n_i n_0 S_i \xi$$

ξ is the energy consumed per ionisation event (ionisation energy + radiation) [2]. Classical parallel electron heat conduction is adopted [1]

$$\chi_{\|,e} = 3.16\frac{T_e \tau_e}{m_e} \qquad \tau_e = \frac{3\sqrt{m_e}}{4\sqrt{2\pi}}\frac{T_e^{\frac{3}{2}}}{\lambda e^4 n} \approx \frac{3.5x10^4}{\lambda/10}\frac{T_e^{\frac{3}{2}}}{n_i}$$

while models for anomalous particle and heat diffusivities are used to describe perpendicular electron transport.

2.3 Equations for Neutrals

2.3.1 General (Coordinate Independent) Form of Neutral Equations

Continuity Equation

$$\frac{\partial n_0}{\partial t} = -\nabla(n_0 \vec{\upsilon}_0) - n_0 n_i S_i \qquad (6)$$

Momentum Equation

$$\frac{\partial}{\partial t}(m n_0 \vec{\upsilon}_0) = -\nabla(n_0 T_0 + n_0 m \vec{\upsilon}_0 \vec{\upsilon}_0) - \vec{R}_{i-n} \qquad (7)$$

Energy Equation

$$\frac{\partial E_0}{\partial t} = -\nabla(n_0 \vec{\upsilon}_0 H_0 - n_0 \chi_0 \nabla T_0) - Q_{0,i} \qquad (8)$$

where

$$H_0 = \frac{3}{2}T_0 + \frac{1}{2}n_0 m \upsilon_0^2$$

2.3.2 Pseudo 2-D Equations for Neutrals

In the very high collisionality regime under consideration perpendicular transport is negligible and all x-dependences can be removed by making the usual 1-D approximation by analogy with the ions. For convenience, we therefore omit all x-dependences in the neutral transport equations from the beginning.

The neutral flow velocity is basically two dimensional. However, because of axysymmetry, quantities depend only on the distance from the plate. As a consequence all equations can be brought into 1-D form. Different from the ions, however, one has to consider separate equations for the transport of perpendicular and toroidal momentum. Perpendicular transport inside a magnetic surface also has to be included.

In the coordinate system $\left(\vec{e}_{\tilde{y}}, \vec{e}_z\right)$ where $\vec{e}_{\tilde{y}}$ is the direction perpendicular to the plate and $\vec{e}_z$ is the direction parallel to the magnetic field, the neutral velocity is defined as

$$\vec{v}_0 = v_{0,\perp}\vec{e}_{\tilde{y}} + v_{0,z}\vec{e}_z \tag{9}$$

In the coordinate system $\left(\vec{e}_{\tilde{y}}, \vec{e}_{\tilde{z}}\right)$ where $\vec{e}_{\tilde{z}}$ is the toroidal direction:

$$\vec{v}_0 = v_{0,\tilde{y}}\vec{e}_{\tilde{y}} + v_{0,\tilde{z}}\vec{e}_{\tilde{z}} \tag{10}$$

When deriving the neutral equations both coordinate systems are used for convenience. Toroidal symmetry leads to:

$$\frac{\partial}{\partial \tilde{z}} = 0, \quad \frac{\partial}{\partial y} = -\frac{\cos\psi}{\sin\psi}\frac{\partial}{\partial z}, \quad \frac{\partial}{\partial \tilde{y}} = \frac{-1}{\sin\psi}\frac{\partial}{\partial z} \tag{11}$$

Continuity Equation

$$\frac{\partial n_0}{\partial t} = -\frac{\partial n_0 v_{0,\tilde{y}}}{\partial \tilde{y}} + \frac{\partial}{\partial x}\left(D_\perp \frac{\partial n_i}{\partial x}\right) - n_0 n_i (S_i - S_{rec})$$

$$= \frac{1}{\sin\psi}\frac{\partial n_0 v_{0,\tilde{y}}}{\partial z} + \frac{\partial}{\partial x}\left(D_\perp \frac{\partial n_i}{\partial x}\right) - n_0 n_i (S_i - S_{rec}) \tag{12}$$

With the definition

$$v_{0,\tilde{y}} = \tilde{v}_0 \sin\psi \tag{13}$$

one gets

$$\frac{\partial n_0}{\partial t} = \frac{\partial n_0 \tilde{v}_0}{\partial z} + \frac{\partial}{\partial x}\left(D_\perp \frac{\partial n_i}{\partial x}\right) - n_0 n_i (S_i - S_{rec}) \tag{14}$$

Neutral Momentum Equation ($\vec{e}_{\tilde{y}}$ Direction)

$$\frac{\partial}{\partial t}\left(mn_0\upsilon_{0,\tilde{y}}\right)=-\frac{\partial}{\partial\tilde{y}}\left(n_0T_0+n_0m\upsilon_{0,\tilde{y}}^2\right)-\frac{\partial}{\partial x}\left(mn_0\upsilon_{0,x}\upsilon_{0,\tilde{y}}\right)-R_{i-n,\tilde{y}} \tag{15}$$

Using Eqs. (11) and (13) and $\upsilon_{i,\tilde{y}}=\upsilon_{i,z}\sin\psi$ one gets for the momentum exchange term

$$\begin{aligned}R_{i-n,\tilde{y}}&=-mn_in_0\left(S_{cx}+\upsilon_t\sigma_{i-n}\right)\left(\upsilon_{0,\tilde{y}}-\upsilon_{i,\tilde{y}}\right)-n_in_0mS_i\upsilon_{0,\tilde{y}}\\&=-mn_in_0\left(S_{cx}+\upsilon_t\sigma_{i-n}\right)\left(\tilde{\upsilon}_0-\upsilon_{i,z}\right)\sin\psi-n_in_0mS_i\tilde{\upsilon}_0\sin\psi\end{aligned} \tag{16}$$

Treating the other terms in the same way yields

$$\begin{aligned}\sin\psi\frac{\partial}{\partial t}\left(mn_0\tilde{\upsilon}_0\right)&=\frac{1}{\sin\psi}\frac{\partial}{\partial z}\left(n_0T_0+n_0m\tilde{\upsilon}_0^2\sin^2\psi\right)+\sin\psi\frac{\partial}{\partial x}\left(m\tilde{\upsilon}_0D_{0,\perp}\frac{\partial n_0}{\partial x}\right)\\&-mn_in_0\left(S_{cx}+\upsilon_t\sigma_{i-n}\right)\left(\tilde{\upsilon}_0+\upsilon_{i,z}\right)\sin\psi-mn_in_0\left(S_i\tilde{\upsilon}_0+S_{rec}\upsilon_{i,z}\right)\sin\psi\end{aligned} \tag{17}$$

Neutral Momentum Equation ($\vec{e}_{\tilde{z}}$ Direction)

The corresponding equation for toroidal momentum is given by

$$\begin{aligned}\frac{\partial}{\partial t}\left(mn_0\upsilon_{0,\tilde{z}}\right)&=-\frac{\partial}{\partial\tilde{y}}\left(n_0m\upsilon_{0,\tilde{y}}\upsilon_{0,\tilde{z}}\right)-mn_in_0\left(S_i\upsilon_{0,\tilde{z}}-S_{rec}\upsilon_{i,\tilde{z}}\right)\\&-mn_in_0\left(S_{cx}+\upsilon_t\sigma_{i-n}\right)\left(\upsilon_{0,\tilde{z}}-\upsilon_{i,\tilde{z}}\right)\end{aligned} \tag{18}$$

where $\frac{\partial}{\partial\tilde{z}}\equiv 0$ has been used. With $\upsilon_{0,\tilde{z}}=-\upsilon_{0,z}\cos\psi$ and $\upsilon_{i,\tilde{z}}=-\upsilon_{i,z}\cos\psi$ one gets

$$\begin{aligned}\frac{\partial}{\partial t}\left(mn_0\upsilon_{0,z}\right)&=\frac{\partial}{\partial z}\left(n_0m\tilde{\upsilon}_0\upsilon_{0,z}\right)-mn_in_0\left(S_i\upsilon_{0,z}-S_{rec}\upsilon_{i,z}\right)\\&-mn_in_0\left(S_{cx}+\upsilon_t\sigma_{i-n}\right)\left(\upsilon_{0,z}-\upsilon_{i,z}\right)\end{aligned} \tag{19}$$

By analogy we can now also give an explicit expression for the momentum source term in the ion equation

$$\begin{aligned}R_{i-n,z}&=\vec{e}_z\cdot\left(mn_in_0\left(S_i\vec{\upsilon}_0-S_{rec}\vec{\upsilon}_i\right)+mn_in_0\left(S_{cx}+\upsilon_t\sigma_{i-n}\right)\left(\vec{\upsilon}_0-\vec{\upsilon}_i\right)\right)\\&=mn_in_0\left(S_i\upsilon_{0,z}-S_{rec}\upsilon_{i,z}\right)-\sin\psi n_in_0mS_i\upsilon_{0,\perp}+n_in_0m\left(S_{cx}+\upsilon_t\sigma_{i-n}\right)\left(\upsilon_{0,z}-\upsilon_{i,z}\right)\end{aligned}$$

$$-n_i n_0 m(S_{cx} + \upsilon_t \sigma_{i-n})(\tilde{\upsilon}_0 + \upsilon_{i,z})\sin^2\psi$$

$$= -mn_i n_0(S_i + S_{cx} + \upsilon_t \sigma_{i-n})(\tilde{\upsilon}_0 + \upsilon_{i,z})\sin^2\psi + mn_i n_0(S_i \upsilon_{0,z} - S_{rec}\upsilon_{i,z})$$

$$+n_i n_0 m(S_{cx} + \upsilon_t \sigma_{i-n})(\upsilon_{0,z} - \upsilon_{i,z}) \qquad (20)$$

Energy Equation

$$\frac{\partial E_0}{\partial t} = \frac{\partial}{\partial z}(n_0 \tilde{\upsilon}_0 H_0) + \frac{1}{\sin^2(\psi)}\frac{\partial}{\partial z}\left(n_0 \chi_0 \frac{\partial T_0}{\partial z}\right) - Q_{0,i} + (x - \text{direction})$$

$$H_0 = \frac{5}{2}T_0 + \frac{1}{2}m\left(\tilde{\upsilon}_0^2 \sin^2(\psi) + \upsilon_i^2 \cos^2(\psi)\right) \qquad (21)$$

2.4 1-D Equations

Following the standard procedure in deriving 1-D equations, model profiles of the form

$$Y(x,z) = Y(z)e^{\lambda_Y x}$$

are assumed for the basic variables with prescribed inverse decay length λ_Y, which may be different for different variables. 1-D equations are then obtained from the equations given in Sec. 3 by performing the integration $\int_0^\infty \ldots dx$, thus assuming the wall to be sufficiently far away from the plasma so that fluxes to the wall can be neglected. (This is a condition that has to be fulfilled in any well designed tokamak and does not pose a real restriction.) For terms which are products of powers of basic variables, the integration is performed explicitly. Otherwise, (this applies mainly to terms containing atomic rate expressions) tabulated profile factors of the form $F(n_i, T_i, T_e, ..) = F(n_{i,0}, T_{i,0}, T_{e,0}, ..)\ Pr_F$ are used, where $_0$ denotes separatrix values. In what follows all variables are taken at the separatrix and $_0$ is omitted for convenience.

Ion Continuity Equation

$$\frac{1}{\lambda_{n_i}}\frac{\partial n_i}{\partial t} = -\frac{1}{\lambda_{n_i} + \lambda_\upsilon}\frac{\partial}{\partial z}(n_i \upsilon_i) + S_n + n_0 n_i S_i\, Pr_{S_i} \qquad (22)$$

where integration by parts yields the particle source across the separatrix into the scrape off layer:

$$S_n = D_\perp \frac{\partial n_i(0)}{\partial x}$$

Ion Momentum Balance

$$\frac{1}{\lambda_{n_i}+\lambda_\upsilon}\frac{\partial m n_i \upsilon_i}{\partial t}$$

$$=-\frac{\partial}{\partial z}\left[\frac{n_i T_e}{\lambda_{n_i}+\lambda_e}+\frac{n_i T_i}{\lambda_{n_i}+\lambda_i}+\frac{n_i m \upsilon_i^2}{\lambda_{n_i}+2\lambda_\upsilon}\right]+1.28\frac{\partial}{\partial z}\left(\frac{n_i T_i \tau_i}{2.5\lambda_i+\lambda_\upsilon}\frac{\partial \upsilon_i}{\partial z}\right)$$

$$-m n_i n_0 \tilde{\upsilon}_0 \sin^2\psi$$

$$\times\left(S_i \, Pr_{n_i n_0 \tilde{\upsilon}_0 S_i}+\frac{S_{cx}}{\lambda_{n_i}+\lambda_{n_0}+\lambda_{\upsilon_0}+0.33\lambda_{T_i}}+\frac{\upsilon_t \sigma_{i-n}}{\lambda_{n_i}+\lambda_{n_0}+\lambda_{\upsilon_0}+0.5\lambda_{T_i}}\right)$$

$$-m n_i n_0 \upsilon_{i,z} \sin^2\psi$$

$$\times\left(S_i \, Pr_{n_i n_0 \tilde{\upsilon}_0 S_i}+\frac{S_{cx}}{\lambda_{n_i}+\lambda_{n_0}+\lambda_{\upsilon_0}+0.33\lambda_{T_i}}+\frac{\upsilon_t \sigma_{i-n}}{\lambda_{n_i}+\lambda_{n_0}+\lambda_{\upsilon_0}+0.5\lambda_{Ti}}\right)$$

$$+m n_i n_0\left(S_i \upsilon_{0,z} \, Pr_{n_i n_0 \upsilon_{0,z} S_i}-S_{rec}\upsilon_{i,z} \, Pr_{n_i n_0 \upsilon_{i,z} S_{rec}}\right)$$

$$+n_i n_0 m \upsilon_{0,z}\left(\frac{S_{cx}}{\lambda_{n_0}+\lambda_{n_i}+\lambda_{\upsilon_0}+0.33\lambda_{T_i}}+\frac{\upsilon_t \sigma_{i-n}}{\lambda_{n_0}+\lambda_{n_i}+\lambda_{\upsilon_0}+0.5\lambda_{T_i}}\right)$$

$$-n_i n_0 m \upsilon_{i,z}\left(\frac{S_{cx}}{\lambda_{n_0}+\lambda_{n_i}+\lambda_\upsilon+0.33\lambda_{T_i}}+\frac{\upsilon_t \sigma_{i-n}}{\lambda_{n_0}+\lambda_{n_i}+\lambda_\upsilon+0.5\lambda_{T_i}}\right) \tag{23}$$

Ion Energy Equation

$$\frac{\partial}{\partial t}\left(\frac{3}{2}\frac{n_i T_i}{\lambda_{n_i}+\lambda_i}+\frac{1}{2}\frac{m n_i \upsilon_i^2}{\lambda_{n_i}+2\lambda_\upsilon}\right)$$

$$=-\frac{\partial}{\partial z}\left[\frac{5}{2}\frac{n_i \upsilon_i T_i}{\lambda_{n_i}+\lambda_e+\lambda_\upsilon}+\frac{1}{2}\frac{m n_i \upsilon_i^3}{\lambda_{n_i}+3\lambda_\upsilon}-\frac{2}{5\lambda_i}n_i \chi_{\|,i}\frac{\partial T_i}{\partial z}\right]$$

$$-\frac{1}{\lambda_{n_i}+\lambda_\upsilon+\lambda_e}\upsilon_i\frac{\partial(n_i T_e)}{\partial z}+Q_i+Q_{\Delta,e}+Q_{0,i} \tag{24}$$

where Q_i is the power flux to the ions across the separatrix.

Electron Temperature Equation

$$\frac{\partial}{\partial t}\left(\frac{\frac{3}{2}n_i T_e}{\lambda_{n_i}+\lambda_e}\right)=-\frac{\partial}{\partial z}\left[\frac{5}{2}\frac{T_e n_i \upsilon_i}{\lambda_{n_i}+\lambda_e+\lambda_\upsilon}-\frac{1}{\frac{5}{2}\lambda_e}n_i\chi_{\|,e}\frac{\partial T_e}{\partial z}\right]$$

$$+\frac{1}{\lambda_{n_i}+\lambda_\upsilon+\lambda_e}\upsilon_i\frac{\partial(n_i T_e)}{\partial z}-Q_{\Delta,e}-n_0 n_i S_i \xi \Pr_{Si\xi}+Q_e \qquad (25)$$

where Q_e is the power flux to the electrons across the separatrix.

Neutral Energy Equation

Integrating Eq. (21) in the x-direction yields

$$\frac{\partial E_0}{\partial t}=\frac{\partial}{\partial z}\left(\frac{5}{2}\frac{n_0\tilde{\upsilon}_0 T_0}{\lambda_{n_0}+\lambda_{\upsilon_0}+\lambda_{T_0}}\right)+\frac{1}{2}\frac{mn_0\tilde{\upsilon}_0^3\sin^2\psi}{\lambda_{n_0}+3\lambda_{\upsilon_0}}+\frac{1}{2}\frac{mn_0\tilde{\upsilon}_0\upsilon_{i,z}^2\cos^2\psi}{\lambda_{n_0}+\lambda_{\upsilon_0}+2\lambda_\upsilon}$$

$$+\frac{1}{\sin^2\psi}\frac{\partial}{\partial z}\left(\frac{n_0\chi_0}{\lambda_{n_0}+\lambda_{T_0}}\frac{\partial T_0}{\partial z}+\frac{5}{2}\frac{n_0\tilde{\upsilon}_0 T_0 D_0}{2\lambda_{n_0}+\lambda_{\upsilon_0}+\lambda_{T_0}}\frac{\partial n_0}{\partial z}+\frac{1}{2}\frac{n_0 m\tilde{\upsilon}_0^3\sin^2\psi}{2\lambda_{n_0}+3\lambda_{\upsilon_0}}\right.$$

$$\left.+\frac{1}{2}\frac{n_0 m\tilde{\upsilon}_0\upsilon_{i,z}^2\cos^2\psi}{2\lambda_{n_0}+\lambda_{\upsilon_0}+2\lambda_{n_0}}\frac{\partial n_0}{\partial z}\right) \qquad (26)$$

Assuming equal temperatures for the ion and neutrals ($T_i = T_0$), the two energy equations can be added into one equation for the total ion and neutral energy.

Continuity Equation Neutrals

$$\frac{1}{\lambda_{n_0}}\frac{\partial n_0}{\partial t}=\frac{1}{\lambda_{n_0}+\lambda_{\upsilon_0}}\frac{\partial n_0\tilde{\upsilon}_0}{\partial z}-n_0 n_i S_i \Pr_{S_i}+n_0 n_i S_{rec}\Pr_{S_{rec}} \qquad (27)$$

Neutral Momentum Equation ($\bar{e}_{\tilde{y}}$ Direction)

$$\sin\psi\frac{1}{\lambda_{n_0}+\lambda_{\upsilon_0}}\frac{\partial}{\partial t}\left(mn_0\tilde{\upsilon}_0\right)$$

$$=\frac{1}{\sin\psi}\frac{\partial}{\partial z}\left(\frac{1}{\lambda_{n_0}+\lambda_{T_i}}n_0 T_0+\frac{1}{\lambda_{n_0}+2\lambda_{\upsilon_0}}n_0 m\tilde{\upsilon}_0^2\sin^2\psi\right)$$

$$-\frac{mn_i n_0 S_{cx}\tilde{\upsilon}_0 \sin\psi}{\lambda_{n_i}+\lambda_{n_0}+0.33\lambda_{T_0}+\lambda_{\upsilon_0}}-\frac{mn_i n_0 \upsilon_t \sigma_{i-n}\tilde{\upsilon}_0 \sin\psi}{\lambda_{n_i}+\lambda_{n_0}+0.5\lambda_{T_0}+\lambda_{\upsilon_0}}$$

$$-\frac{mn_i n_0 S_{cx}\upsilon_{i,z} \sin\psi}{\lambda_{n_i}+\lambda_{n_0}+0.33\lambda_{T_i}+\lambda_{\upsilon}}-\frac{mn_0 n_e \upsilon\sigma_{i-n}\upsilon_{i,z} \sin\psi}{\lambda_{n_i}+\lambda_{n_0}+0.5\lambda_{T_i}+\lambda_{\upsilon}}$$

$$-mn_i n_0\left(S_i\tilde{\upsilon}_0 \Pr_{mn_0 n_i S_i\tilde{\upsilon}_0}+S_{rec}\upsilon_{iz}\Pr_{mn_i n_0 S_{rec}\upsilon_{i,z}}\right)\sin\psi \tag{28}$$

Neutral Momentum Equation ($\vec{e}_{\tilde{z}}$ Direction)

$$\frac{1}{\lambda_{n_0}+\lambda_{\upsilon_0}}\frac{\partial}{\partial t}\left(mn_0\upsilon_{0,z}\right)=\frac{1}{\lambda_{n_0}+2\lambda_{\upsilon_0}}\frac{\partial}{\partial z}\left(n_0 m\tilde{\upsilon}_0\upsilon_{0,z}\right)$$

$$-mnn_0\left(S_i\upsilon_{0,z}\Pr_{nn_0 S_i\upsilon_{0,z}}-S_{rec}\upsilon_{i,z}\Pr_{nn_0 S_{rec}\upsilon_{0,z}}\right)$$

$$-mnn_0 S_{cx}\left(\frac{\upsilon_{0,z}}{\lambda_n+\lambda_{n_0}+0.33\lambda_{T_i}+\lambda_{\upsilon_0}}-\frac{\upsilon_{i,z}}{\lambda_n+\lambda_{n_0}+0.33\lambda_{T_i}+\lambda_{\upsilon}}\right)$$

$$-mnn_0\upsilon_t\sigma_{i-n}\left(\frac{\upsilon_{0,z}}{\lambda_{n_i}+\lambda_{n_0}+0.5\lambda_{T_i}+\lambda_{\upsilon_0}}-\frac{\upsilon_{i,z}}{\lambda_n+\lambda_{n_0}+0.5\lambda_{T_i}+\lambda_{\upsilon}}\right) \tag{29}$$

The same decay length is assumed for the poloidal and toroidal neutral velocities $\tilde{\upsilon}_0$ and $\upsilon_{0,z}$, respectively.

2.5 Boundary Conditions

The boundary conditions for the fluid model are not obvious and little information can be found in literature. This is, in particular, true of the ion momentum equation and the neutral fluids in general, if realistic surface physics is taken into account. We therefore confine our analysis to the limiting cases of perfectly reflecting and perfectly absorbing walls, where the physics is relatively clear. Ad hoc models for the intermediate cases are implemented in the code, but will not be described in this report.

In the relations given in this Section all quantities are to be taken at the plate (x = L).

2.5.1 Perfectly Reflecting Plate

In this subsection the limit of a perfectly reflecting plate is considered (specular reflection). For practical purposes an ad hoc model for imperfect reflection is included by introducing particle and energy reflection coefficients R_N and R_E, respectively as described in Appendix 3. (The perfectly reflecting limit corresponds to $R_N = R_E = 1$.)

In what follows sheath related expressions are taken from Refs. [3, 4]. The sheath

potential, in particular is given by

$$e\phi_f = \frac{1}{2} T_e \ln\left[2\pi \frac{m_e}{m} \left(1 + \frac{T_i}{T_e} \right) (1 - \gamma_e)^{-2} \right] \tag{30}$$

where γ_e is the secondary electron emission coefficient.

Ion Particle Balance

Free outflow of ions

$$\Gamma = n v_z \tag{31}$$

with the constraint (Bohm condition at the plate)

$$v \geq c_s = \sqrt{\frac{\gamma T_i + T_e}{m}} \tag{32}$$

Neutral Particle Balance

The flux of incoming neutrals is equal to the outgoing ion flux

$$\tilde{\Gamma}_0 = \Gamma_{0,\tilde{y}} / \sin\psi = \Gamma R_N \tag{33}$$

Electron and Ion Energy Balances

For the electron and ion energy balances the expressions for the electron and ion sheath transmission factors of Ref. 4 are taken.

$$q_e = \left(\frac{2T_e}{1 - \gamma_e} - e\phi_f \right) \Gamma \tag{34}$$

$$q_i = \left(\frac{m}{2} v_z^2 + \frac{5}{2} T_i \right) \Gamma \tag{35}$$

These are essentially the fluid expressions for free outflow of energy into the sheath region, modified by the effects of secondary electron emission and the sheath field.

Neutral Energy Balance

The energy flux by neutrals from the plate must be equal to the ion energy flux to the plate. However, the energy gain of the ions in the sheath potential has to be added to the value at the sheath entrance as given by Eq. (35).

$$\tilde{q}_0 \equiv n_0 \tilde{v}_0 H_0 = \frac{n_0 v_{0,\tilde{y}} H_0}{\sin\psi} = R_E\left(\frac{m}{2} v_z^2 + \frac{5}{2} T_i - e\phi_f\right)\Gamma = R_E(q_i - e\phi_f)\Gamma \tag{36}$$

Momentum Balance Ions

Free outflow of ion momentum

$$\Pi_i = mnv_z^2 \tag{37}$$

Momentum Balance Neutrals

The boundary condition for the poloidal component of the momentum equation is obtained from the requirement that the neutral momentum flux from the plate in the normal direction equals the normal ion momentum flux to the plate. However, since our plate quantities are actually taken at the sheath entrance, the momentum gain in the sheath has to be added to the ion momentum at the sheath entrance. In a very simple way the momentum gain is estimated from the gain of a single particle in the sheath field given by Eq. (30). This yields

$$\sin^2\psi \tilde{T}_0 \equiv m n_0 \tilde{v}_0^2 \sin^2\psi = m\Gamma \sin\psi \tilde{v}_{0,\tilde{y}} =$$

$$= m\Gamma \sin\psi v_z \sqrt{1 - \frac{2ne\Phi_f f_{inc}}{mv_z^2}} \sin\psi = mnv_z^2 \sqrt{1 - \frac{2ne\Phi_f}{mv_z^2}} \sin^2\psi \tag{38}$$

where the prescribed parameter $f_{inc} < 1$ crudely takes into account that the ions do not hit the plate in normal direction [4].

The case of the toroidal component of the momentum equation is treated in exactly the same way.

2.5.2 Perfectly Absorbing Plate

It is assumed that ions **and** neutrals hitting the wall are transferred into cold neutrals which are recycled at some distance d away from the plate with zero energy and momentum and a prescribed spatial source distribution. Under these conditions one has free outflow of particles, energy and momentum for both ions and neutrals.

Ion Particle Balance

Free outflow of ions

$$\Gamma = nv_z \tag{39}$$

with the constraint (Bohm condition at the plate)

$$\upsilon \geq c_s = \sqrt{\frac{\gamma T_i + T_e}{m}} \tag{40}$$

Neutral Particle Balance

Free outflow of neutrals

$$\tilde{\Gamma}_0 = n_0 \tilde{\upsilon}_0 \tag{41}$$

Electron and Ion Energy Balances

For the electron and ion energy balances the expressions for the electron and ion sheath transmission factors of Ref. 4 are taken.

$$q_e = \left(\frac{2T_e}{1-\gamma_e} - e\phi_f \right) \Gamma \tag{42}$$

$$q_i = \left(\frac{m}{2} \upsilon_z^2 + \frac{5}{2} T_i \right) \Gamma \tag{43}$$

Neutral Energy Balance

Free outflow of neutral energy

$$\tilde{q}_0 = n_0 \tilde{\upsilon}_0 H_0 \tag{44}$$

Momentum Balance Ions

Free outflow of ion momentum

$$\Pi_i = mn\upsilon_z^2 \tag{45}$$

Momentum Balance Neutrals

Free outflow of ion momentum

$$\sin^2 \psi \Pi_0 = \sin^2 \psi mn\upsilon_z^2 \tag{46}$$

The artificial source for the recyling of the cold neutrals is then given by

$$S_{0,slow} = S(\Gamma - \Gamma_0) \tag{47}$$

where S is a normalised shape function.

3. DESCRIPTION OF THE NUMERICAL SCHEME

3.1 Introduction

The main objective of the SOL-One code is to solve the equations with the appropriate boundary conditions along a field line in the scrape-off layer as discussed in the previous chapters. The solution consists of the full time dependence of the variables from the initial conditions to steady state. To enable the study of different models and boundary conditions, the code should allow for an easy implementation of the equations in the code.

The time scales of the physics in the scrape-off layer vary over many orders of magnitude. For the numerical solution of the equation with respect to time one can use either an explicit or an implicit scheme. With an explicit numerical scheme, (where the information of the new time depends only on data from previous time points), it is necessary to resolve the smallest time scale. This requires a very small time step and consequently many time steps to reach steady state. The advantage of an explicit scheme is that each time step can be computed relatively fast and the memory requirements are modest. For the solution of our one-dimensional equations we use an implicit scheme. This allows much larger time steps and consequently requires much fewer time steps. The memory requirements are not prohibitive for our one-dimensional problem.

The spatial length scales of the solution of the SOL equations vary from a few centimetres close to the target plate to typically many meters in the upstream region. To resolve these scale lengths efficiently requires a flexible placement of grid points. Isoparametric finite elements are well suited for this. The boundary conditions of the SOL equations at the target plate usually take the form of an expression for the outflowing flux, which are natural boundary conditions. Using finite elements for the representation of the solution allows for an elegant implementation of these natural conditions.

3.2 Numerical Method

3.2.1 Petrov-Galerkin Finite Elements [6]

The SOL equations as described in Section 3 are of the convection-diffusion type:

$$M\frac{\partial U}{\partial t} = A\frac{\partial U}{\partial x} - D\frac{\partial^2 U}{\partial^2 x} \tag{48}$$

where U is a vector containing the variables and M, A and D are the coefficient matrices.

The usual Galerkin weak form of Eq. (48) is obtained by multiplying with a weight function $\upsilon(x)$ and integrating over the domain of interest:

$$\int \upsilon(x) M \frac{\partial U(x)}{\partial t} dx = \int \upsilon(x) \left(A \frac{\partial U}{\partial x} - D \frac{\partial^2 U}{\partial^2 x} \right) dx \tag{49}$$

Integration by parts of the diffusion term replaces the second derivative in U(x) with a single derivative in $\upsilon(x)$ and creates a boundary term. The boundary term can be used to implement the natural boundary conditions, i.e. specifying of the flux instead of the value of U at the boundaries.

$$\int \upsilon(x) M \frac{\partial U(x)}{\partial t} dx = \int \upsilon(x) A \frac{\partial U}{\partial x} + \frac{\partial \upsilon}{\partial x} D \frac{\partial U}{\partial x} dx - \left[\upsilon D \frac{\partial U}{\partial x} \right]_0^L \tag{50}$$

The function U(x) is numerically represented with (isoparametric) finite elements. The elements are defined in a local coordinate r which runs from -1 to +1. Both the function U and the space coordinate x are represented with the same finite elements, so-called isoparametric finite elements.

$$U(r) = \sum u_i h(r), \quad x(r) = \sum x_i h(r) \tag{51}$$

where u_i are the expansion coefficients and h(r) the finite elements. Here we will use linear finite elements, with the function h(r) defined as

$$\begin{array}{lll} h(r) = 1 - r_0 r & r_0 = -1 & \text{for } -1 < r < 0 \\ & r_0 = 1 & \text{for } 0 < r < 1 \end{array} \tag{52}$$

For standard Galerkin finite elements the functions $\upsilon(r)$ are the same as the finite elements h(r) used in the representation of U. However, in the case that the diffusion is much smaller than the convection (i.e. large Peclet numbers) standard Galerkin finite elements (FE) (as well as finite differences) can lead to non-physical oscillations in the space coordinate. These oscillations occur mostly due to badly resolved boundary layers in the solution. One of the simplest ways to resolve this problem is the use of weight functions $\upsilon(r)$ which are not identical to the shape functions h(r), so-called Petrov Galerkin finite elements. This scheme is similar to upwind finite differences (but not identical to). One choice of weight function is:

$$\upsilon(r) = h(r) + \alpha \frac{\partial h}{\partial r} \tag{53}$$

In this way more weight is given to downstream information. For the simple equation (48) an optimum value for α can be derived:

$$\alpha_{opt} = \frac{P_e}{|P_e|} \coth|P_e| - \frac{1}{|P_e|} \tag{54}$$

where P_e is the numerical Peclet number defined as:

$$P_e = \frac{A(x_i - x_{i-1})}{2D} \tag{55}$$

The choice $\alpha = 1$ leads to a full upwind scheme. In case A and D are functions of x, the local value of P_e is to be used. The integrations in Eq. (50) are performed numerically using a two-point Gaussian integration method. This is of sufficient accuracy, i.e. it does not degrade the accuracy of the solution.

3.2.2 Implicit Time Stepping

For the time evolution of the system of equations, an implicit scheme has been chosen. This allows the time step to be much larger that the smallest time scale present in the system, i.e. Courant numbers much larger than unity are allowed. Especially as the system approaches steady state very large time steps are possible. Another advantage is that the time scale on which the time evolution is accurately approximated can be chosen by setting the maximum time step smaller than the time scale of interest. Typically one is not interested in the very short time scales, of, for example, the parallel electron diffusion time but more in the time scale of a change in the sources or in the boundary conditions typically of the order of milliseconds.

The (non-linear) SOL system can be written in matrix form as:

$$\frac{\partial \mathbf{U}}{\partial t} = \mathbf{H}(\mathbf{U}, t) \tag{56}$$

The generalised trapezoidal method is used for the time evolution of Eq. (56) [7]:

$$\mathbf{U}^{n+1} - \mathbf{U}^n = \Delta t\left(\theta \mathbf{H}^{n+1} + (1-\theta)\mathbf{H}^n\right) \tag{57}$$

For $\theta = 0.5$ the method is known as the Crank-Nicholson scheme (or the trapezoidal rule). This scheme is second order accurate in time. However **H** is a non-linear function of the variable U and needs to be linearised.

$$\mathbf{H}^{n+1} = \mathbf{H}\left(\mathbf{U}^{n+1}\right) = \mathbf{H}^n + \left(\frac{\partial \mathbf{H}}{\partial \mathbf{U}}\right)\left(\mathbf{U}^{n+1} - \mathbf{U}^n\right) + O\left(\Delta t^2\right) \tag{58}$$

Combining (57) and (58) gives the scheme used in the SOL-One code:

$$\left(1 - \theta\Delta \frac{\partial \mathbf{H}\left(\mathbf{U}^n\right)}{\partial \mathbf{U}}\right)\Delta \mathbf{U}^n = \Delta t \mathbf{H}^n \tag{59}$$

In practice, the SOL equations are not given in the form of Eq. (56) but rather in the form:

$$\frac{\partial \mathbf{B}(\mathbf{U})}{\partial t} = \mathbf{A}(\mathbf{U}, x) \tag{60}$$

Using $\partial \mathbf{B} / \partial t = (\partial \mathbf{B} / \partial \mathbf{U})(\partial \mathbf{U} / \partial t)$ Eq. (59) can be written as:

$$\left(\frac{\partial \mathbf{B}(\mathbf{U}^n)}{\partial \mathbf{U}} - \theta \Delta t \frac{\partial \mathbf{A}(\mathbf{U}^n)}{\partial \mathbf{U}} \right) \Delta \mathbf{U}^n = \Delta t \mathbf{A}^n \tag{61}$$

where $\Delta \mathbf{U}_n = \mathbf{U}_{n+1} - \mathbf{U}_n$. Thus at every time step a system of linear equations in $\Delta \mathbf{U}_n$ has to be solved. The matrices are non-symmetric and are of the block-diagonal form. The width of the diagonal is 3 times the number of equations. The system of equations is solved using Gaussian elimination. Some preconditioning of the matrix is essential due to the wide range of numerical values that the different variables can assume, i.e. density $10^{13}cm^{-3}$ and temperatures of 1-100eV. At present the matrix and the vector are preconditioned by dividing by the value on the diagonal of the matrix.

3.2.3 Numerical Evaluation of the Jacobian

The equations implemented in the SOL-One code are highly non-linear. Linearising the equations analytically would be very cumbersome. Also, it would not allow for an easy change or extension of the equations. Therefore, at the cost of some cpu time, the linearisation of the equations is done numerically. This requires that each equation is split into two parts; one part of the equation which is integrated by parts and the remaining part that is not. The linearisation is done with respect to both the variable and its derivative as independent variables. The equations are therefore written in terms of the seven variables and their derivatives.

3.2.4 Boundary Conditions

The number of boundary conditions that have to be specified for each equation depends on the characteristics of the equations at the boundary of the computational domain. At present, our computational domain is one divertor leg, from the symmetry point where the velocity and density and temperature gradients are zero to the outflow point at the sheath entrance at the plate. For the momentum equation the boundary condition at the symmetry point is given (by definition) by $v_i = 0$. At the sheath entrance, the velocity is set to Mach 1 or larger. This is implemented by first calculating, at each time step, the value of the velocity with free streaming boundary conditions in the momentum equation. If this value is smaller than Mach 1, the solution is recalculated with Mach 1 as a boundary condition. (Note that this hardly increases the cpu time, the dominant factor in the cpu time is the evaluation of the two matrices A and B of (61)). For the continuity equation, with no inflow and only supersonic outflow, no boundary conditions can be specified. The upstream density cannot be specified as a boundary

condition but will be determined by the source rate in the continuity equation. In the two energy equations, the outstreaming energy flux has to be specified. This is a natural boundary condition. Integration by parts of the diffusive terms of the weak form of the energy equations creates a boundary term which allows specification of the energy fluxes in terms of any combination of variables. In the continuity and perpendicular momentum equations for the neutrals, there is an incoming flux of neutrals from the plate which has to be specified, i.e. both the neutral density and the perpendicular neutral velocity at the plate have to be specified. The toroidal neutral momentum also has an incoming flux of momentum. This requires the specification of the neutral toroidal momentum at the plate.

3.2.5 Variable Time Stepping

The maximum time step that can be taken in the implicit scheme implemented in the SOL-One code is not limited by a CFL condition. Rather, the maximum time step is determined by the non-linear stability of the scheme. In practice, the time step is optimised at every iteration in time such that the maximum change in any of the variables is less than 50% of the average value. This requires several solutions (with a maximum of typically five) of the system of linear equations at each step in time. A maximum value of the time step has to be introduced as the system approaches steady state and the changes in the variables become small at each iteration. A typical value for the maximum time step is 10ms.

3.3 Code Validation

In this section, the numerical properties of the code are discussed. As an example we calculate the steady state solution of a typical case. The table below shows the input parameters used for this case. The behaviour of the time step as a function of the iteration number is shown in Fig. 2. Also shown is the maximum change of the variables. As discussed in the previous paragraph, initially the value of the time step is adjusted such that the relative change is fixed at 50%. After iteration n = 28 the maximum value of the time step is reached and the relative change drops to a very small value when steady state is reached. After the initial fast evolution of the initial conditions at time steps of 0.1μs, the system rapidly approaches steady state after typically 10ms. The steady state solution of the seven variables is shown in Fig. 3.

The convergence of the solution with the number of finite elements is shown in Fig. 4. It shows the error in the ion continuity and the ion momentum equation. The error in the equation is seen to decrease linearly with the number of finite elements. The scaling is linear because the weak form of the equations contains first derivatives. Linear finite elements give a linear approximation for the derivatives. The error in the variables will scale quadratically with the number of finite elements. Fig. 5 shows the convergence of the boundary condition of the electron energy flux. This is a natural boundary condition which is satisfied with an accuracy which scales with the number of grid points. The flux can be calculated from either

$\Gamma_e = \chi_e \nabla T_e$ or from $\Gamma_e = \gamma_e n_i v_i$. As can be seen from Fig. 5, the error in the flux not containing any derivatives scales quadratically with the finite element size, the error in the flux with the first derivative scales linearly.

Parameters used for Convergence Study		
Parameter	**Value**	**Units**
Field line length	2640	cm
Field line angle with target	0.05	rad
Total heating to electrons	2.5	MW
Total heating to ions	2.5	MW
Upstream density (feedback)	1.6×10^{13}	cm^{-3}
Electron energy transmission coefficient	4.5	
Ion energy transmission coefficient	2.5	
Perpendicular scale length	0.66	cm^{-1}

4. APPLICATION TO DETACHMENT IN A STATIC GAS TARGET DIVERTOR [8]

Experimentally, detachment is usually approached by increasing the density at otherwise fixed plasma parameters. On most devices detachment is a gradual process, which exhibits a rollover of the ion saturation current I_{sat}^{+}, followed by a gradual decrease. Simultaneously, the D_α signal increases and the divertor pressure decreases by an order of magnitude at basically unchanged or moderately changing upstream conditions.

In a static gas target (i.e. the model as described in the previous sections) the ion-neutral mean free path is small compared to the scrape-off layer width and the momentum losses of the neutrals to the walls is small. In this case the ion pressure gradient has to be balanced by the neutral pressure gradient.

In this section, the potential of a static gas target to provide a drop in plasma pressure along the magnetic field is investigated.

4.1 Time Evolution during Density Ramp

The detachment of a static gas target is modelled with the SOL-One code by introducing a constant source rate of particles in the upstream region. Starting from a steady state solution, the particle source is turned on and the SOL equations are solved as a function time. The parameters used in the calculation are the same as for the test case in Section 5 (see Table, Section 5). The source rate is such that the upstream density rises from $6 \times 10^{12} cm^{-3}$ to

$1.2 \times 10^{13} cm^{-3}$ in one second.

Fig. 6 shows the time evolution of the ion density, the electron temperature and the ion pressure profile. At t = 0.5s, the electron and ion temperatures drop to a low value of about 1eV. At the same time, the pressure in the divertor, which is rising at earlier times, starts to drop (detachment). The upstream pressure is increasing all the time except when detachment begins, where the upstream is constant (or even slightly decreasing) for a short time.

4.2 Steady State Solutions

Alternatively, the detachment can be studied through a series of steady state solutions in which the upstream density is set to a predetermined value. To obtain this present value a feedback scheme is used on the upstream source rate. The results obtained this way are similar to the results from the time dependent problem of the previous paragraph.

Fig. 7 shows the density and electron temperatures in the divertor as a function of the total particle content N_{tot}. The upstream density increases monotonically with N_{tot}. The divertor electron temperature falls rapidly with increasing particle content up to the point of detachment (at a particle content larger than 7×10^{16}). For higher densities the divertor temperature decreases only slightly. Generally, after detachment the divertor quantities tend to saturate while the upstream density and pressure increase linearly with the total particle content. This indicates that the additional particles accumulate in the upstream region. The pressure drop is therefore caused by an increasing upstream pressure at constant divertor pressure, not by a reduction of the divertor pressure.

The particle flux towards the target, which is a measure of the ion saturation current, is plotted in Fig. 8. Contrary to what is observed experimentally, the particle flux in our model is not decreasing after detachment but levels off to a constant value at high density.

Examples of the high recycling solution at low density and of a typical detached solution are shown in Figs. 9a and 9b respectively.

7. CONCLUSIONS

The fluid equations in the scrape-off layer for ions, electrons and neutrals along the magnetic field lines have been successfully implemented in the numerical code SOL-One. The combination of Petrov-Galerkin finite elements and a fully implicit scheme for the time evolution yields a very robust code. Steady state solutions are typically obtained with less than 50 iterations (time steps). The cpu requirements are low, so that the code can be used interactively.

As an initial application, the problem of detachment in a static gas target divertor has been studied. With increasing density, the model does show momentum detachment with a divertor temperature below one eV, but typically experimental observations, in particular the drop of

I_{sat}^{+}, are not reproduced.

REFERENCES

[1] BRAGINSKII, S.I., in Reviews of Plasma Physics, Vol. 1 (Leontovich, M.A., Ed.), Consultants Bureau, New York (1965).

[2] HARRISON, M.F.A., et al., Nucl. Technol./Fusion 3 (1983) 432.

[3] STANGEBY, P.C., in Physics of Plasma-Wall Interactions in Controlled Fusion (POST, D.E., BEHRISCH, R., Eds), NATO ISI Series B, Vol. 131, Plenum Press, New York and London (1986) 41.

[4] CHODURA, R., in Physics of Plasma-Wall Interactions in Controlled Fusion (POST, D.E., BEHRISCH, R., Eds), NATO ISI Series B, Vol. 131, Plenum Press, New York and London (1986) 99.

[5] JANEV, R.K. et al., Elementary Processes in Hydrogen-Helium Plasma, Springer Verlag, Berlin (1987).

[6] ZIENKIEWICZ, O.C., and TAYLOR, R.L., "The Finite Element Method", Volume 2, McGraw-Hill, UK (1989).

[7] HIRSCH, C., "Numerical Computation of Internal and External Flows", Volume 1, John Wiley and Sons, Chichester, U.K. (1988).

[3] BORRASS, K. and HUYSMANS, G.T.A., "Investigation of Momentum Detachment in a Static Gas Target", Proc. 22nd European Conf. on Controlled Fusion and Plasma Physics, Bournemouth, p.341, (1995).

APPENDIX I

General Expressions

In this appendix units are cgs units, except for T which is in eV. μ is the mass number.

The Coulomb Logarithm [1]

$T_e < 50eV$:

$$\lambda = 23.4 - 1.15^{10} \log n_i + 3.45^{10} \log T_e$$

$Te > 50eV$:

$$\lambda = 25.3 - 1.15^{10} \log n_i + 2.33^{10} \log T_e$$

Charge Exchange Reaction Rate

$$S_{cx} = 9.28325 \times 10^{-9} T_i^{0.33}$$

Elastic Ion-Neutral Collision Cross-Section

$$\sigma_{ei} = 5.0 \times 10^{-15}$$

The Thermal Ion Velocity

$$\upsilon_{T_i} = 9.79 \times 10^5 \sqrt{\frac{T_i}{\mu}}$$

APPENDIX II

Atomic Physics

Different models are used to describe the hydrogen atomic physics, depending on the required accuracy and the processes involved.

A simple analytical model is used in the regime where recombination is negligible and atomic processes are not dominant. This model basically relies on Ref. [2]. Units are cgs units, except for T_e, which is in eV.

Hydrogen Ionisation Rate

$$S_i = S_i^0[1 + \frac{10}{T_e}\left(\frac{n}{10^{14}}\right)^{p0}]$$

$$p0 = 0.5\left(1 - 1.36\bar{e}^{n/10^{13}}\right)$$

$$S_i^0 = 10^{-6}e^{-(p1+13.82)}$$

$$p1 = (((((-9.94\times10^{-5}\ \log(T_e) + 4.5\times10^{-3})\log(T_e) + 7.43\times10^{-2})\log(T_e)$$

$$+.705)\log(T_e) - 3.83)\log(T_e) + 11.4)\log(T_e) - 31.74$$

Mean Energy Per Ionisation Event

$$\xi = 17.5 + \left(5.0 + \frac{37.5}{T_e}\right)^{10}\log\left(\frac{10^{15}}{n_i}\right)$$

In general, data from Ref. [5] are used. The full model is always applied in the evaluation of profile factors. The main reason for using the analytical model is a noticeable saving in computation time.

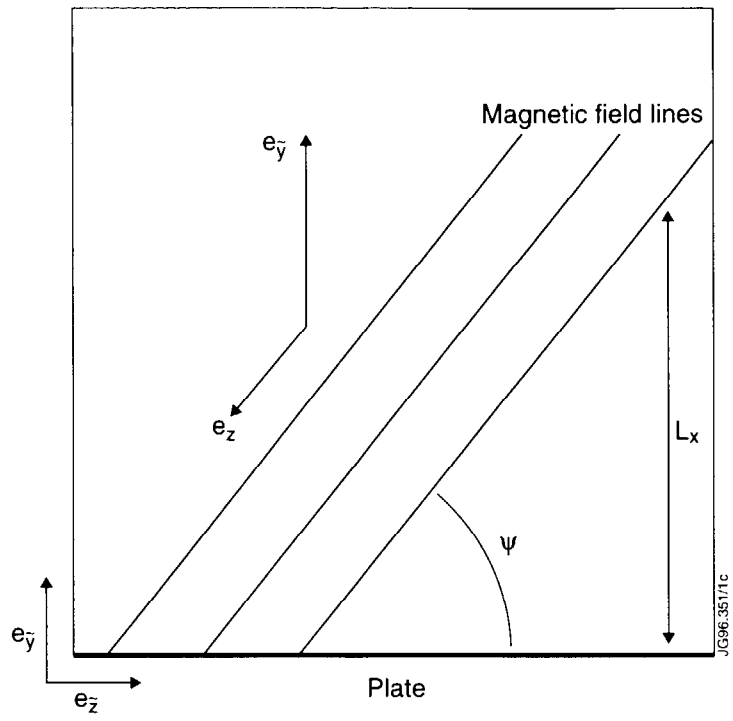

Fig. 1 Basic geometry and coordinates used.

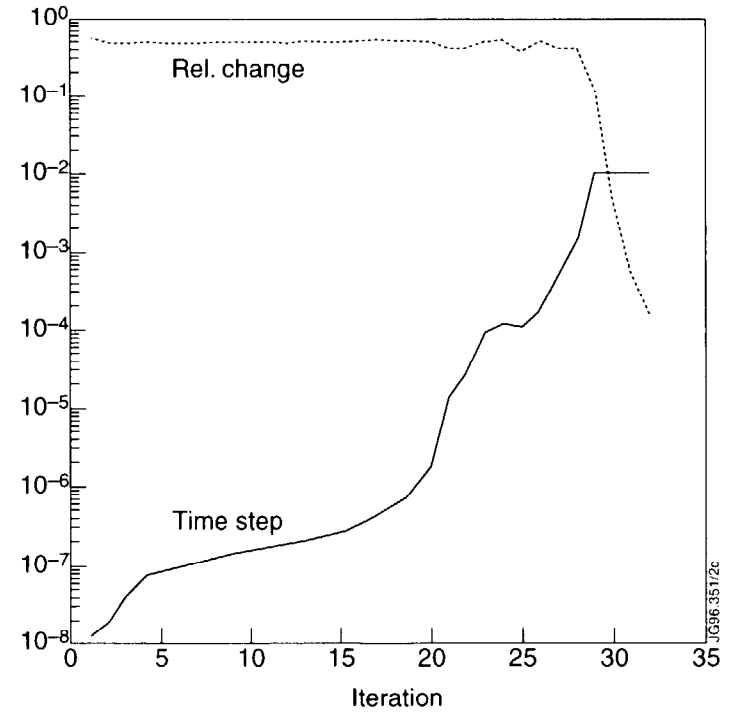

Fig. 2 The value of the time step as a function of the iteration. Also shown is the maximum change in the solution at each iteration.

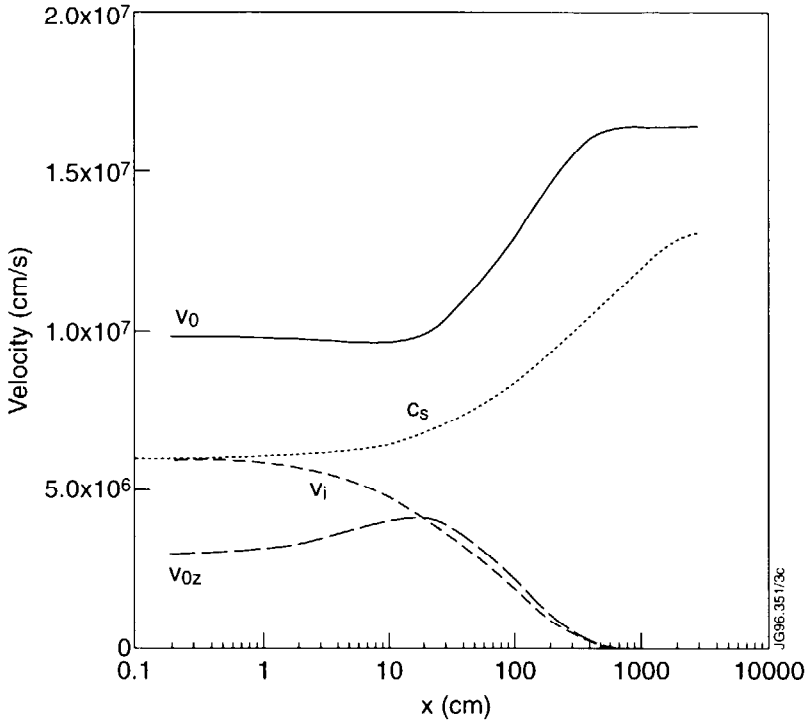
2.0x10^7
1.5x10^7
1.0x10^7
5.0x10^6
0
Velocity (cm/s)
v0
cs
vi
v0z
0.1
1
10
100
1000
10000
x (cm)
JG96.351/3c

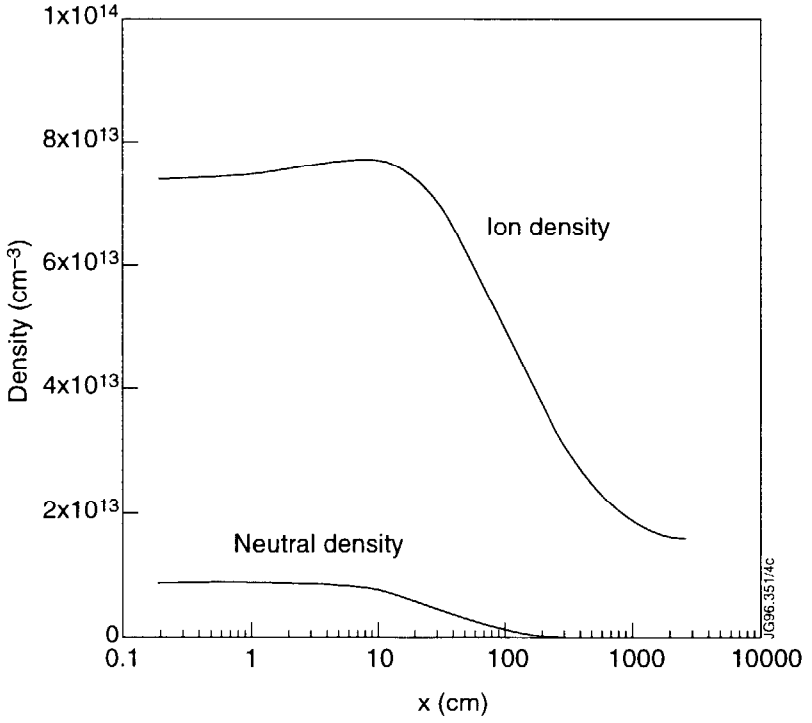
1x10^14
8x10^13
6x10^13
4x10^13
2x10^13
0
Density (cm^-3)
Ion density
Neutral density
0.1
1
10
100
1000
10000
x (cm)
JG96.351/4c

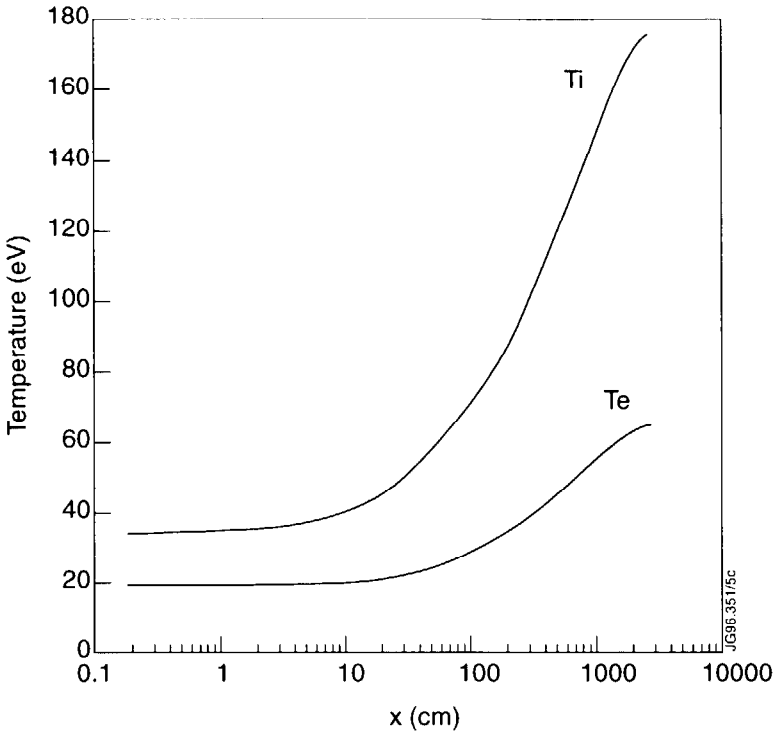

Fig. 3 A typical steady state solution; shown are the seven variables used in the SOL-One code. The sound speed is also displayed.

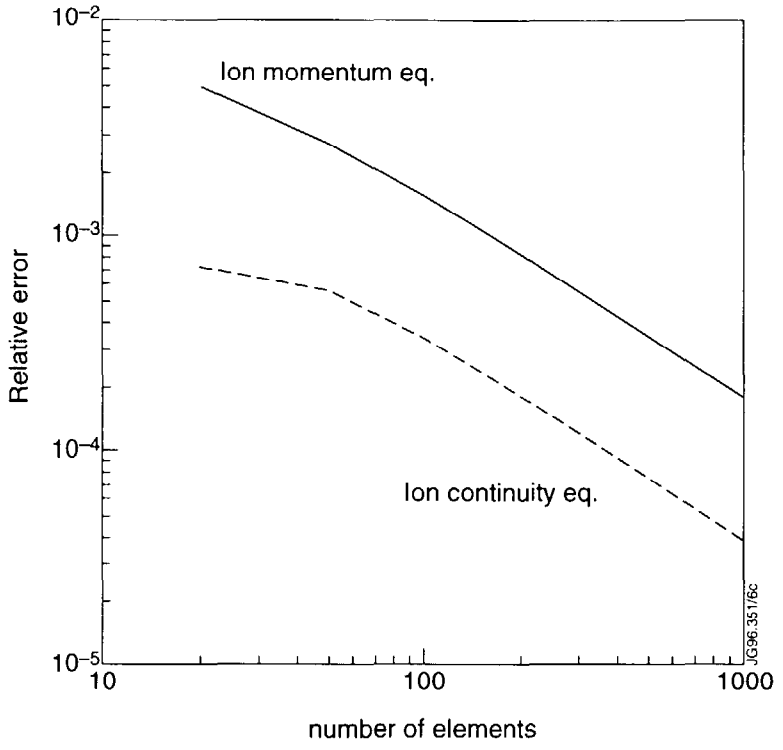

Fig. 4 The error in the ion continuity equation and the ion momentum equation as a function of the number of finite elements.

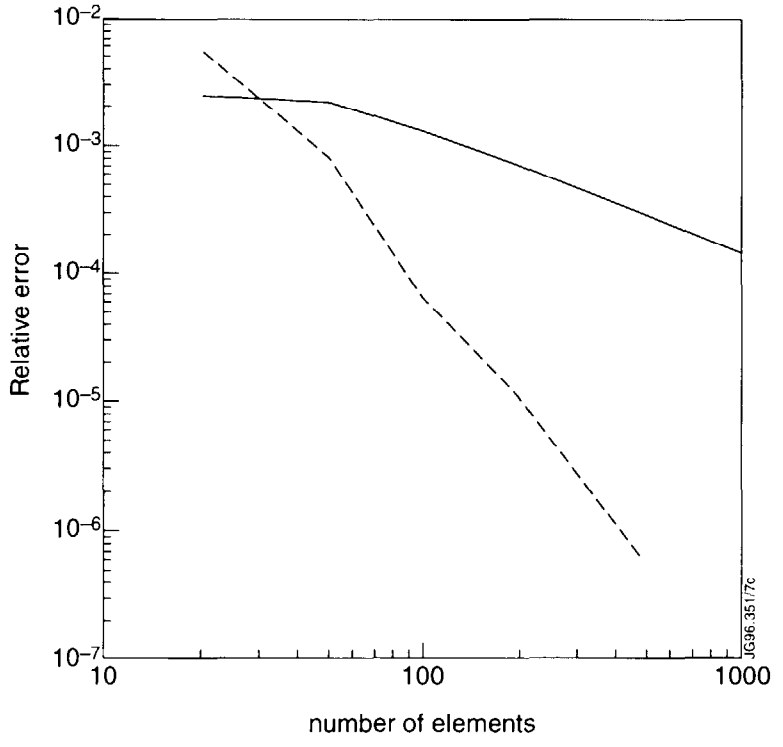

Fig. 5 The error in the value of the electron energy flux at the plate as a function of the number of grid points. The small symbols (upper curve) shows the error in the flux calculated from $\Gamma_e = \chi_e \nabla T_e$. *The large symbols represent the error in the flux calculated from* $\Gamma_e = \gamma_e n_i v_i$.

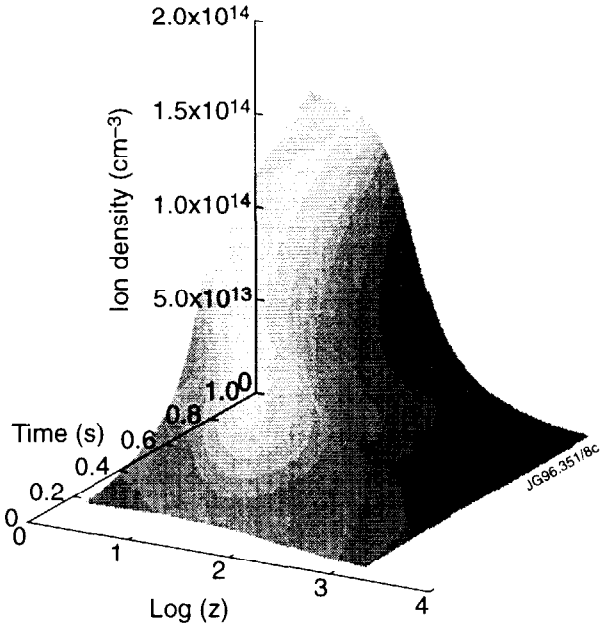

Fig. 6a The time evolution of the electron temperature profile during a density ramp with a constant upstream source. The target is z = 0.

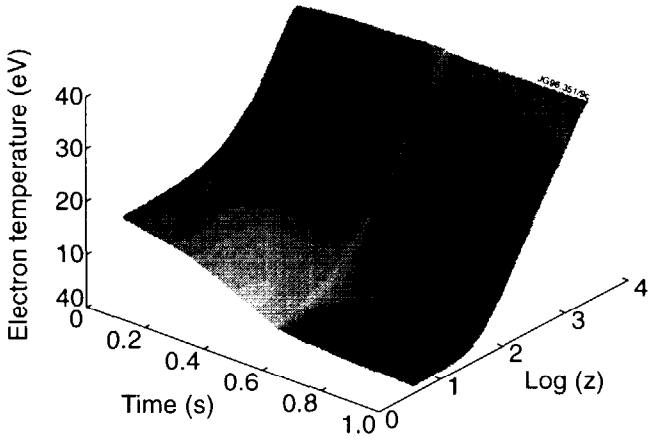

Fig. 6b The time evolution of the electron temperature profile during a density ramp with a constant upstream source.

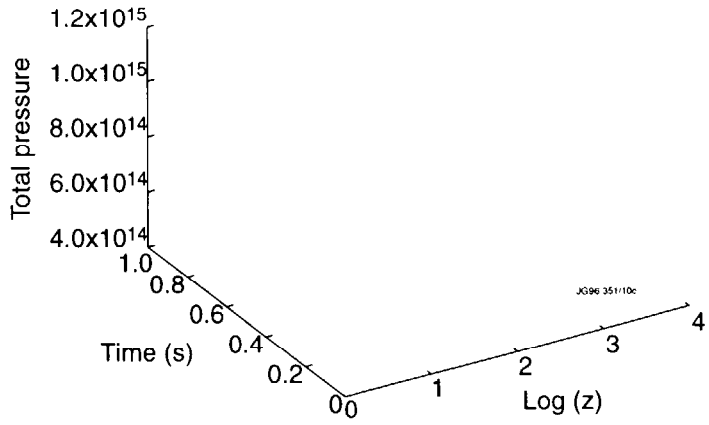

Fig. 6c The time evolution of the pressure profile during a density ramp with a constant upstream source.

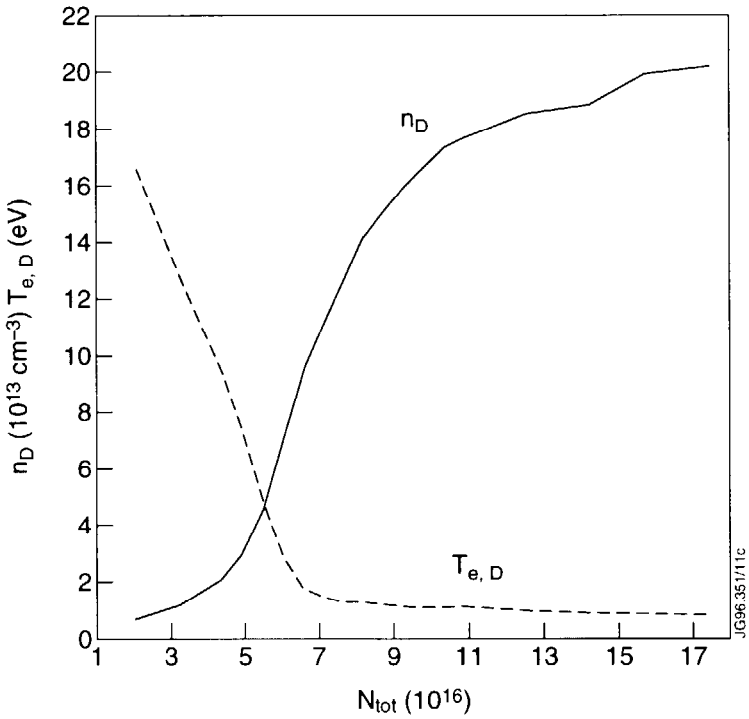

Fig. 7 The divertor density and temperature as a function of the total particle content.

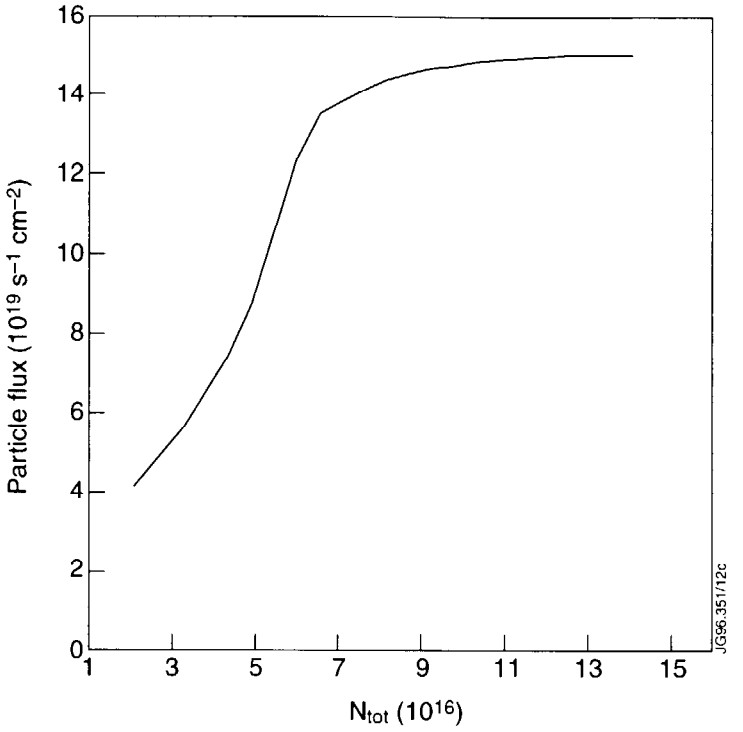

Fig. 8 The particle flux to the target, which is proportional to the ion saturation current, as a function of the total particle content.

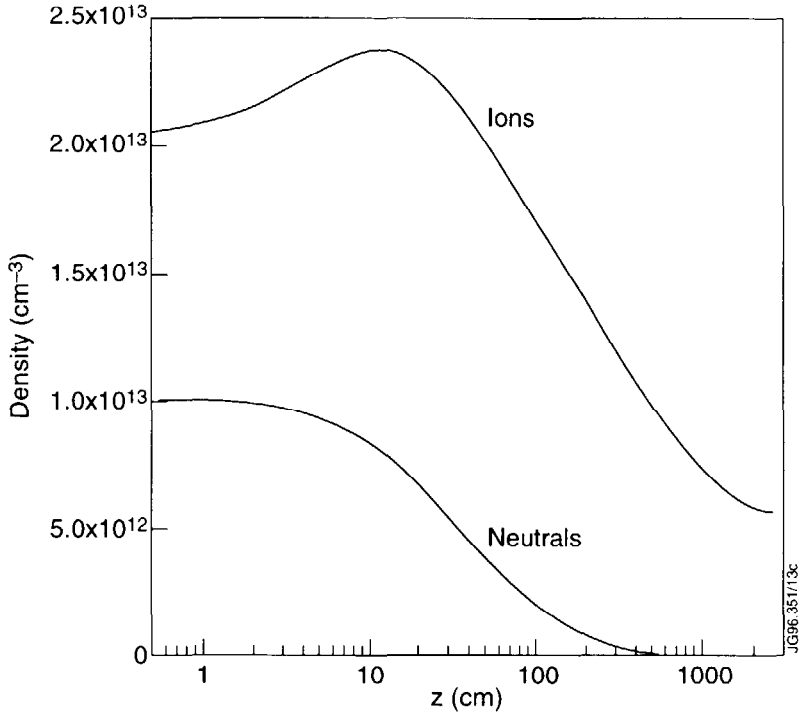
2.5x10^13
2.0x10^13
1.5x10^13
1.0x10^13
5.0x10^12
0
Density (cm^-3)
Ions
Neutrals
1
10
100
1000
z (cm)
JG96.351/13c

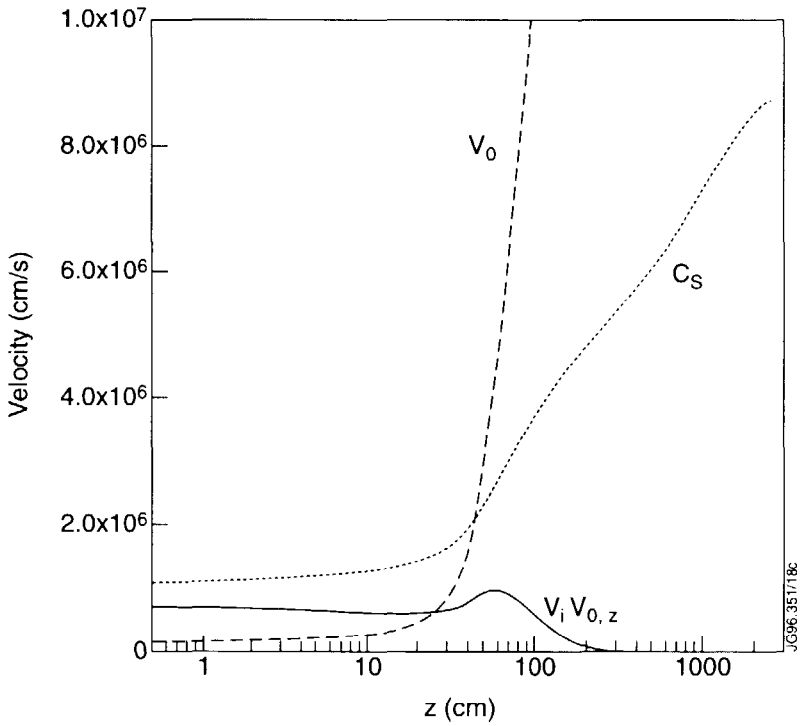
1.0x10^7
8.0x10^6
6.0x10^6
4.0x10^6
2.0x10^6
0
Velocity (cm/s)
V0
Cs
Vi V0, z
1
10
100
1000
z (cm)
JG96.351/18c

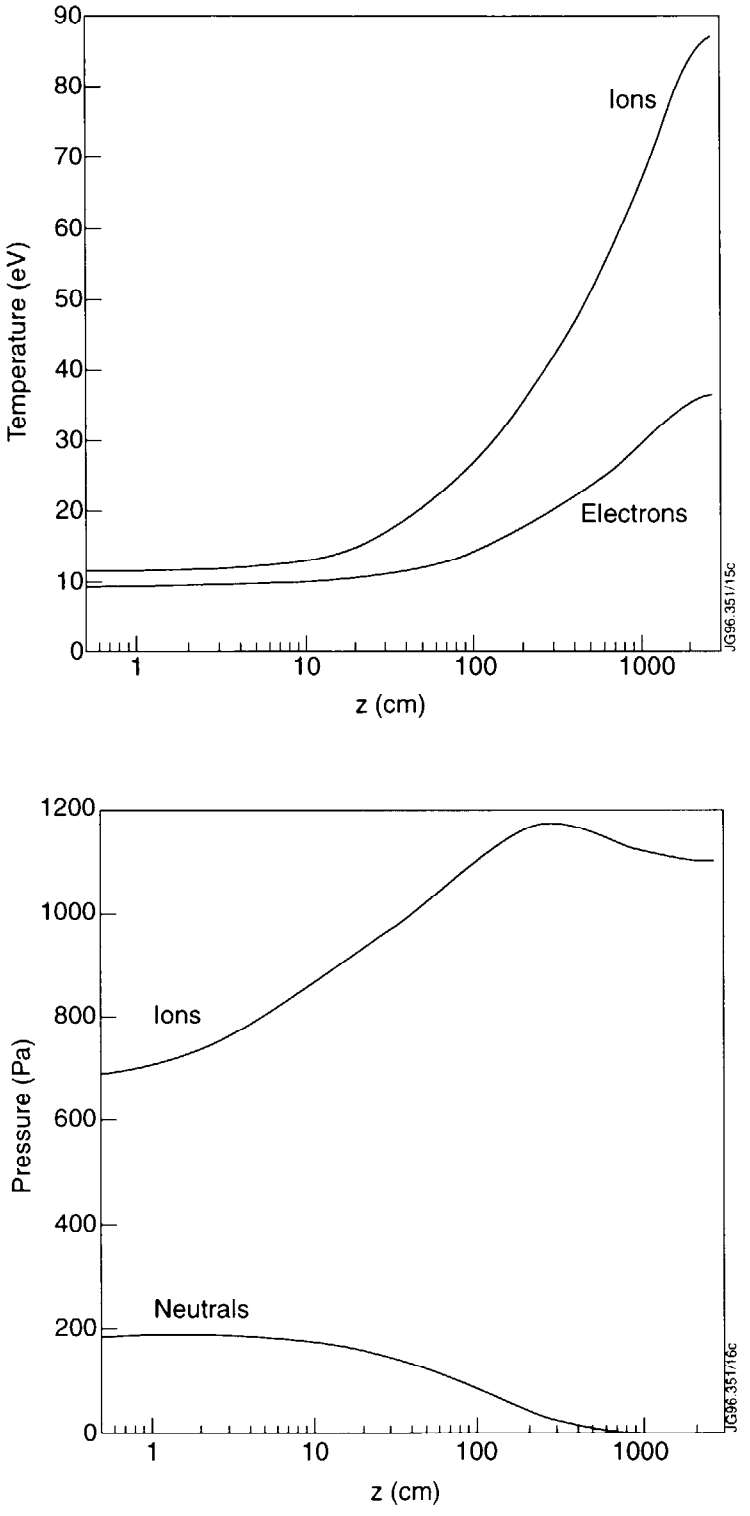

Fig 9a The high recycling (steady state) solution at low density with a high divertor temperature and a low neutral density.

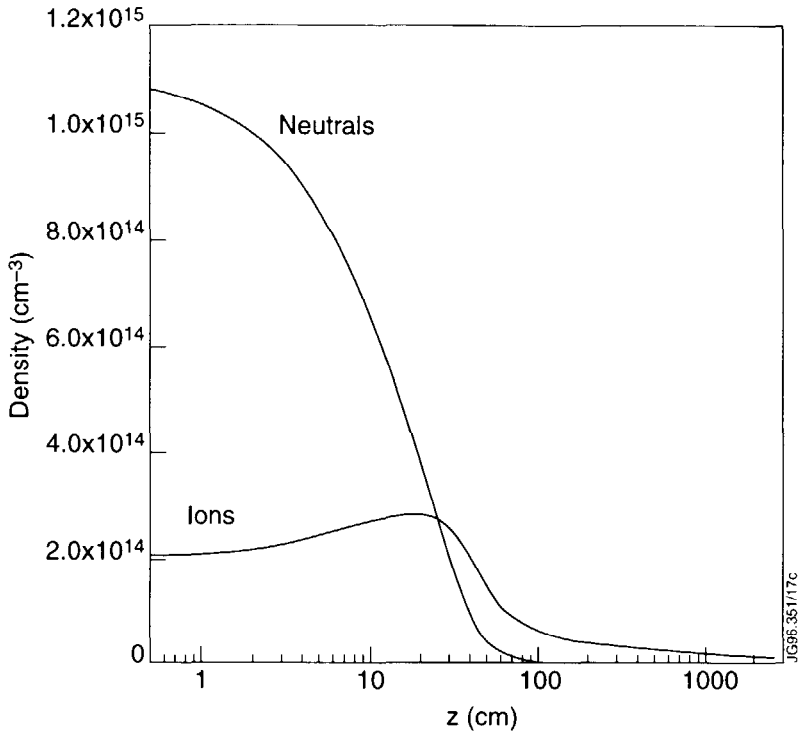
1.2x10^15
1.0x10^15
8.0x10^14
6.0x10^14
4.0x10^14
2.0x10^14
0
Density (cm^-3)
Neutrals
Ions
1
10
100
1000
z (cm)
JG96.351/17c

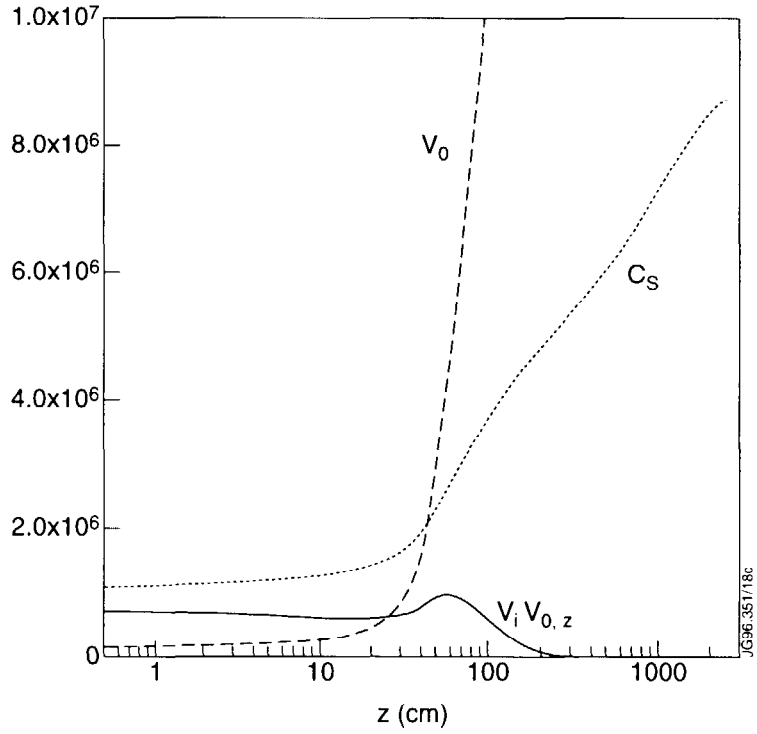
1.0x10^7
8.0x10^6
6.0x10^6
4.0x10^6
2.0x10^6
0
V0
CS
Vi V0, z
1
10
100
1000
z (cm)
JG96.351/18c

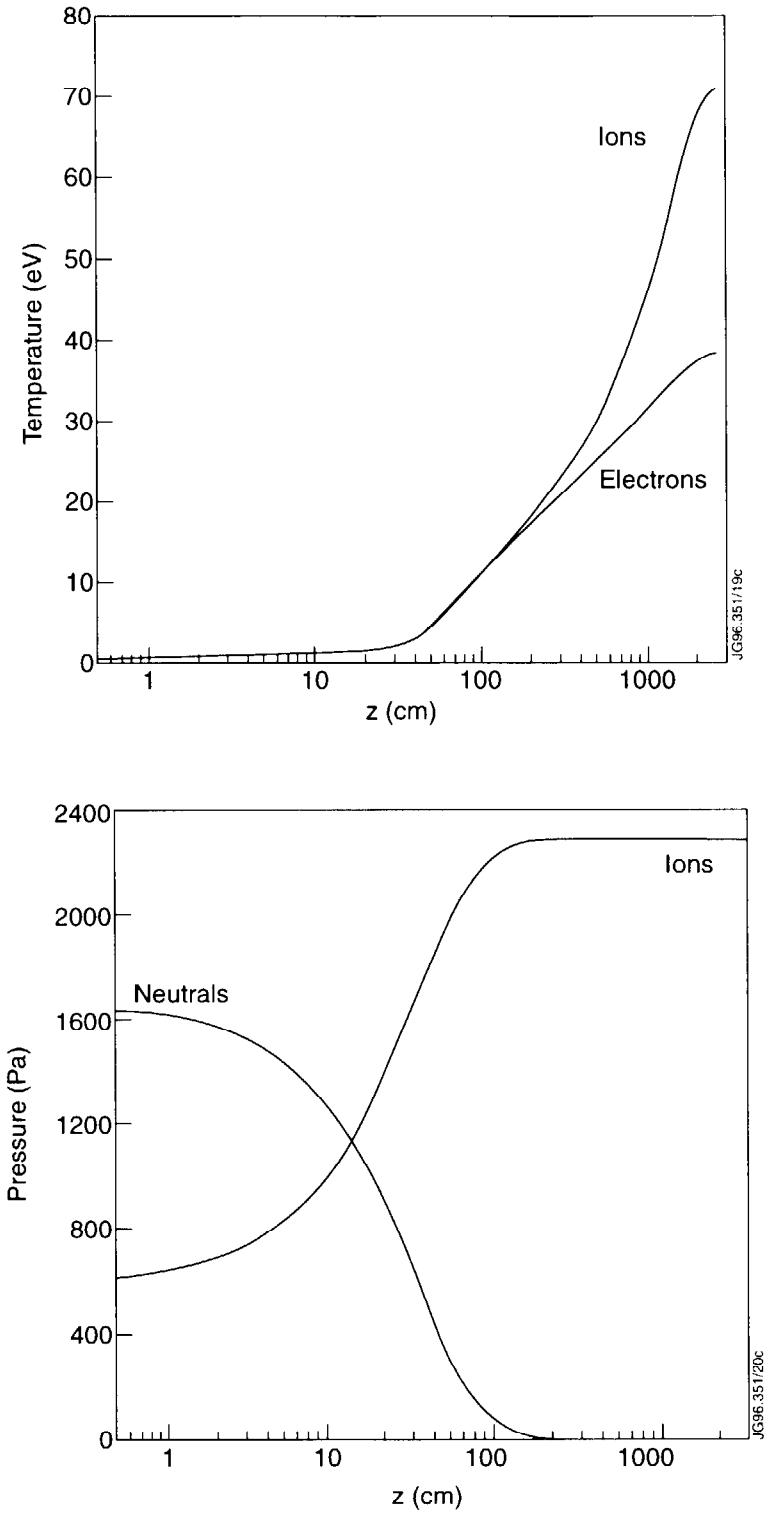

Fig. 9b The (steady state) detached solution at high density with a low divertor temperature and a high neutral density in the divertor.